2009-01

Spatial, Temporal, and Spectral Aspects of Far-Field Radar Data

Cheney, Margaret; Borden, Brett

Spatial, Temporal, and Spectral Aspects of Far-Field Radar Data

Margaret Cheney
Department of Mathematical Sciences
Rensselaer Polytechnic Institute
Troy, NY 12180

Brett Borden
Physics Department
Naval Postgraduate School
Monterey, CA 93943-5001

***Abstract*— We develop a linearized imaging theory that combines the spatial, temporal, and spectral aspects of scattered waves. We consider the case of fixed sensors and a general distribution of objects, each undergoing linear motion; thus the theory deals with imaging distributions in phase space. We derive a model for the data that is appropriate for any waveform, and show how it specializes to familiar results when the targets are far from the antennas and narrowband waveforms are used.**

We use a phase-space imaging formula that can be interpreted in terms of filtered backprojection or matched filtering. For this imaging approach, we derive the corresponding point-spread function. Special cases of the theory reduce to: a) Range-Doppler imaging, b) Inverse Synthetic Aperture Radar (ISAR) and Spotlight Synthetic Aperture Radar (SAR), c) Diffraction Tomography or Ultra-narrowband imaging, and d) Tomography of Moving Targets.

I. Introduction

It is well-known [4], [8] that radar systems can measure both range and velocity of a target, and the resolution in range and velocity depends, via the radar ambiguity function, on the waveform used. Ambiguity-function-based range-Doppler imaging appears at the bottom plane in Fig. 1. Most SAR imaging systems, on the other hand, use a sequence of high-range-resolution pulses, transmitted from a diversity of spatial positions, to form an image of stationary targets. SAR and ISAR, which are closely related, appear on the back plane of Fig. 1. It is also possible to use a sequence of high-Doppler-resolution pulses, transmitted from a diversity of spatial positions, to form an image [2] of stationary targets. Such Doppler SAR techniques appear on the left side of Fig. 1. This diagram suggests the question "What is in the middle of the diagram? How can we combine the spatial, temporal, and spectral aspects of radar data?"

Below we develop a theory that shows how to unify these different imaging approaches. In the process, we will demonstrate how we can fuze the spatial, temporal, and spectral aspects of scattered-field-based imaging. For simplicity, we consider only the far-field case, the general case being published elsewhere [3]. The present discussion deals with the case of fixed distributed sensors, although our results include monostatic configurations (in which a single transmitter and receiver are co-located) as a special case. Methods for imaging stationary scenes in the case when the transmitters and receivers are located at different positions have been particularly well-developed in the geophysics literature [1] and have also been explored in the radar literature [10], [11], [12].

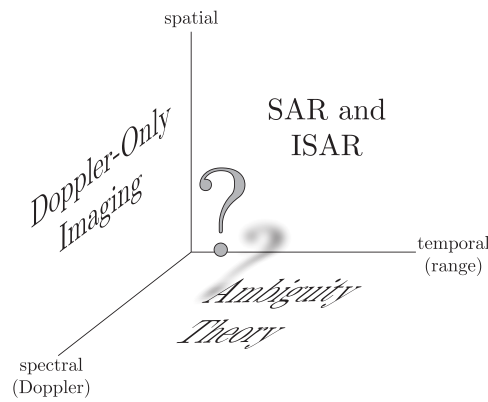

Fig. 1. A diagram of various theories that combine spatial, spectral, and temporal aspects of scattered waves.

II. Model for Data

We model wave propagation and scattering by the scalar wave equation for the wavefield $\psi(t,\boldsymbol{x})$ due to a source waveform $s(t,\boldsymbol{x})$ transmitted at time $-T_{\boldsymbol{y}}$ from location $\boldsymbol{y}$:

$$[\nabla^2 - c^{-2}(t,\boldsymbol{x})\partial_t^2]\psi(t,\boldsymbol{x},\boldsymbol{y}) = \delta(\boldsymbol{x}-\boldsymbol{y})s_{\boldsymbol{y}}(t+T_{\boldsymbol{y}})\,. \quad (1)$$

For simplicity, we consider only localized isotropic sources; the work can easily be extended to more realistic antenna models [9].

A single scatterer moving at velocity $\boldsymbol{v}$ corresponds to an index-of-refraction distribution $n^2(\boldsymbol{x}-\boldsymbol{v}t)$:

$$c^{-2}(t,\boldsymbol{x}) = c_0^{-2}[1+n^2(\boldsymbol{x}-\boldsymbol{v}t)]\,, \quad (2)$$

where c_0 denotes the speed in the stationary background medium (here assumed constant). For radar, c_0 is the speed of light in vacuum. We write $q_{\boldsymbol{v}}(\boldsymbol{x}-\boldsymbol{v}t) = c_0^{-2}n^2(\boldsymbol{x}-\boldsymbol{v}t)$. To model multiple moving scatterers, we let $q_{\boldsymbol{v}}(\boldsymbol{x}-\boldsymbol{v}t)\,d^3x\,d^3v$ be the corresponding quantity for the scatterers in the volume $d^3x\,d^3v$ centered at $(\boldsymbol{x},\boldsymbol{v})$. In other words, q is a distribution in *phase space*, and $q_{\boldsymbol{v}}$ is the spatial distribution, at time $t=0$, of scatterers moving with velocity $\boldsymbol{v}$. Consequently, the scatterers in the spatial volume d^3x (at $\boldsymbol{x}$) give rise to

$$c^{-2}(t,\boldsymbol{x}) = c_0^{-2} + \int q_{\boldsymbol{v}}(\boldsymbol{x}-\boldsymbol{v}t)\,d^3v\,. \quad (3)$$

We note that the physical interpretation of $q_{\boldsymbol{v}}$ involves a choice of a time origin. A choice that is particularly appropriate, in view of our assumption about linear target velocities, is a time during which the wave is interacting with targets of interest. This implies that the activation of the antenna at $\boldsymbol{y}$ takes place at a negative time which we denote by $-T_{\boldsymbol{y}}$. The wave equation corresponding to (3) is then

$$\left[\nabla^2 - c_0^{-2}\partial_t^2 - \int q_{\boldsymbol{v}}(\boldsymbol{x}-\boldsymbol{v}t)\, d^3v\, \partial_t^2\right]\psi(t,\boldsymbol{x}) = s_{\boldsymbol{y}}(t+T_{\boldsymbol{y}})\delta(\boldsymbol{x}-\boldsymbol{y})\,. \quad (4)$$

With the Born (single-scattering) approximation and far-field approximation, the he scattered field can be written [3]

$$\psi_{\rm f}^{\rm sc}(t,\boldsymbol{z},\boldsymbol{y}) = \int \frac{\ddot{s}_{\boldsymbol{y}}\left[\phi(\boldsymbol{x},\boldsymbol{v})\right]}{(4\pi)^2|\boldsymbol{z}||\boldsymbol{y}|} q_{\boldsymbol{v}}(\boldsymbol{x})\, d^3x\, d^3v \quad (5)$$

where

$$\phi(\boldsymbol{x},\boldsymbol{v}) = \alpha_{\boldsymbol{v}}\left(t - |\boldsymbol{z}|/c + \hat{\boldsymbol{z}}\cdot\boldsymbol{x}/c\right) - |\boldsymbol{y}|/c + \hat{\boldsymbol{y}}\cdot\boldsymbol{x}/c + T_{\boldsymbol{y}} \quad (6)$$

and where α denotes the Doppler scale factor

$$\alpha_{\boldsymbol{v}} = \frac{1+\widehat{\boldsymbol{y}}\cdot\boldsymbol{v}/c}{1-\widehat{\boldsymbol{z}}\cdot\boldsymbol{v}/c} \quad (7)$$

In the case when $|\boldsymbol{v}|/c \ll 1$, we have $\alpha_{\boldsymbol{v}} \approx 1 + (\hat{\boldsymbol{y}}+\hat{\boldsymbol{z}})\cdot\boldsymbol{v}/c$.

To write (5) as a Fourier Integral Operator, we write $s_{\boldsymbol{y}}(t)$ in terms of its inverse Fourier transform:

$$s_{\boldsymbol{y}}(t) = \frac{1}{2\pi}\int e^{-i\omega' t} S_{\boldsymbol{y}}(\omega)\, d\omega'\,. \quad (8)$$

We note that by the Paley-Weiner theorem, S is analytic since it is the inverse Fourier transform of the finite-duration waveform s. With (8), we convert (5) into

$$\psi_{\rm f}^{\rm sc}(t,\boldsymbol{z},\boldsymbol{y}) = \int \frac{(-i\omega)^2}{(4\pi)^2|\boldsymbol{z}||\boldsymbol{y}|}\exp\Big(-i\omega\left[\phi(\boldsymbol{x},\boldsymbol{v})\right]\Big) S_{\boldsymbol{y}}(\omega)\, d\omega q_{\boldsymbol{v}}(\boldsymbol{x})\, d^3x\, d^3v. \quad (9)$$

III. Image Formation

The corresponding imaging operation is a filtered version of the formal adjoint of the "forward" operator $\mathcal{F}$. Thus we form the phase-space image $I(\boldsymbol{p},\boldsymbol{u})$ as

$$I_\infty(\boldsymbol{p},\boldsymbol{u}) = \int e^{i\omega[\phi(\boldsymbol{p},\boldsymbol{u})]} Q_\infty(\omega,\boldsymbol{p},\boldsymbol{u},\boldsymbol{z},\boldsymbol{y})\, d\omega\, \psi^{\rm sc}(t,\boldsymbol{z},\boldsymbol{y})\, dt\, d^nz\, d^my. \quad (10)$$

The specific choice of filter is dictated by various considerations [1], [13]; here we make choices that connect the resulting formulas with familiar theories. We take the filter to be

$$Q_\infty(\omega,\boldsymbol{p},\boldsymbol{u},\boldsymbol{z},\boldsymbol{y}) = -(4\pi)^2\omega^{-2}|\boldsymbol{z}||\boldsymbol{y}|S^*_{\boldsymbol{y}}(\omega)J(\omega,\boldsymbol{p},\boldsymbol{u},\boldsymbol{z},\boldsymbol{y})\alpha_{\boldsymbol{u}}\,, \quad (11)$$

which leads (below) to the matched filter. Here the star denotes complex conjugation, and J is a geometrical factor [3] that depends on the configuration of transmitters and receivers.

IV. Analysis of the Point-Spread Function

We obtain the point-spread function of the imaging system by substituting (9) into (10). We thus obtain an image

$$I_\infty(\boldsymbol{p},\boldsymbol{u}) = \int K_\infty(\boldsymbol{p},\boldsymbol{u};\boldsymbol{x},\boldsymbol{v}) q_{\boldsymbol{v}}(\boldsymbol{x}) d^3x d^3v \quad (12)$$

Many radar systems use a narrowband waveform, which is of the form

$$s_{\boldsymbol{y}}(t) = \tilde{s}_{\boldsymbol{y}}(t)\, e^{-i\omega_{\boldsymbol{y}}t} \quad (13)$$

where $\tilde{s}(t,\boldsymbol{y})$ is slowly varying, as a function of t, in comparison with $\exp(-i\omega_{\boldsymbol{y}}t)$, where $\omega_{\boldsymbol{y}}$ is the carrier frequency for the transmitter at position $\boldsymbol{y}$. For the narrowband case, we write $K_\infty^{\rm (NB)}$ instead of K_∞.

In the narrowband case, the point-spread function reduces to [3]

$$K_\infty^{\rm (NB)}(\boldsymbol{p},\boldsymbol{u};\boldsymbol{x},\boldsymbol{v}) = -\int \omega_{\boldsymbol{y}}^2 e^{i\Phi_{\boldsymbol{y},\boldsymbol{z}}}\tilde{J}(\boldsymbol{p},\boldsymbol{u},\boldsymbol{z},\boldsymbol{y}) A_{\boldsymbol{y}}\Big(k_{\boldsymbol{y}}(\hat{\boldsymbol{y}}+\hat{\boldsymbol{z}})\cdot(\boldsymbol{u}-\boldsymbol{v}),\ (\hat{\boldsymbol{z}}+\hat{\boldsymbol{y}})\cdot(\boldsymbol{x}-\boldsymbol{p})/c\Big)\, d^nz\, d^my\,, \quad (14)$$

where $\tilde{J}$ is a geometrical factor closely related to J above, where

$$A_{\boldsymbol{y}}(\tilde{\omega},\tau) = e^{-i\omega_{\boldsymbol{y}}\tau}\int \tilde{s}^*_{\boldsymbol{y}}(t-\tau)\, \tilde{s}_{\boldsymbol{y}}(t)\, e^{i\tilde{\omega}t}\, dt\,. \quad (15)$$

is the narrowband ambiguity function (which is defined here to include a phase) and where

$$e^{i\Phi_{\boldsymbol{y},\boldsymbol{z}}(\boldsymbol{x},\boldsymbol{v},\boldsymbol{p},\boldsymbol{u})} = \exp\left[i(\tilde{\varphi}_{\boldsymbol{x},\boldsymbol{v}} - \tilde{\varphi}_{\boldsymbol{p},\boldsymbol{u}})\right] \exp\left(-ik_{\boldsymbol{y}}(\beta_{\boldsymbol{u}}-\beta_{\boldsymbol{v}})(\hat{\boldsymbol{z}}+\hat{\boldsymbol{y}})\cdot\boldsymbol{x}\right) \quad (16)$$

with $k_{\boldsymbol{y}} = \omega_{\boldsymbol{y}}/c$, $\beta_{\boldsymbol{v}} = (\hat{\boldsymbol{y}}+\hat{\boldsymbol{z}})\cdot\boldsymbol{v}/c$, and

$$\begin{aligned}\tilde{\varphi}_{\boldsymbol{x},\boldsymbol{v}} - \tilde{\varphi}_{\boldsymbol{p},\boldsymbol{u}} &= \frac{\omega_{\boldsymbol{y}}}{c}\left[\left[(1+\beta_{\boldsymbol{u}})\hat{\boldsymbol{z}}+\hat{\boldsymbol{y}}\right]\cdot\boldsymbol{p} - \left[(1+\beta_{\boldsymbol{v}})\hat{\boldsymbol{z}}+\hat{\boldsymbol{y}}\right]\cdot\boldsymbol{x}\right] \\ &= k_{\boldsymbol{y}}\left[(\hat{\boldsymbol{z}}+\hat{\boldsymbol{y}})\cdot(\boldsymbol{p}-\boldsymbol{x}) + \hat{\boldsymbol{z}}\cdot(\beta_{\boldsymbol{u}}\boldsymbol{p}-\beta_{\boldsymbol{v}}\boldsymbol{x})\right]\end{aligned} \quad (17)$$

The narrowband result (14) clearly exhibits the importance of the bistatic bisector vector $\hat{\boldsymbol{y}}+\hat{\boldsymbol{z}}$.

V. Reduction to Special Cases

A. Range-Doppler Imaging

We specialize to the case of range-doppler imaging by using a single transmitter and coincident receiver; in this case the point-spread function reduces to the classical radar ambiguity function [4], [8].

B. High-Range-Resolution Imaging

We recover SAR and ISAR by using high range-resolution (HRR) pulses, for which the ambiguity function is a narrow ridge extending along the ν axis. In these cases, we write

$$A_{\boldsymbol{y}}(\nu,\tau) = \overline{A}_{\boldsymbol{y}}(\tau), \quad (18)$$

with $\overline{A}_{\boldsymbol{y}}(\tau)$ sharply peaked around $\tau = 0$. This ambiguity function together with appropriate relative motion between sensor and target reduces to SAR and ISAR.

C. Diffraction Tomography

Diffraction tomography, which is also called *ultra-narrowband imaging*, uses a single frequency waveform $s(t) = \exp(-i\omega_0 t)$ (with $\tilde{s} = 1$) to interrogate a stationary object. In this case the data is

$$\psi^{\infty}_{\omega_0}(t, \boldsymbol{z}, \boldsymbol{y}) \approx \frac{e^{-ik_0 t}}{(4\pi)^2 |\boldsymbol{z}||\boldsymbol{y}|} F_\infty(\hat{\boldsymbol{y}}, \hat{\boldsymbol{z}})\,, \qquad (19)$$

where the (Born-approximated) *far-field pattern* or *scattering amplitude* is

$$F_\infty(\hat{\boldsymbol{y}}, \hat{\boldsymbol{z}}) = \int e^{-ik_0(\hat{\boldsymbol{z}}+\hat{\boldsymbol{y}})\cdot \boldsymbol{x}} q(\boldsymbol{x})\, d^3x\,. \qquad (20)$$

and where $k_0 = \omega_0/c$. We note that our incident-wave direction convention (from target to transmitter) is the opposite of that used in the classical scattering theory literature (which uses transmitter to target).

Our inversion formula is (10), where there is no integration over t. The resulting formula is

$$I_{k_0}(\boldsymbol{p}) = \int e^{ik_0(\hat{\boldsymbol{z}}+\hat{\boldsymbol{y}})\cdot \boldsymbol{p}}\, Q_{k_0}(\hat{\boldsymbol{z}}, \hat{\boldsymbol{y}}) F_\infty(\hat{\boldsymbol{y}}, \hat{\boldsymbol{z}})\, d\hat{\boldsymbol{y}}\, d\hat{\boldsymbol{z}} \qquad (21)$$

where Q_{k_0} is the filter [5], [6]

$$Q_{k_0} = \frac{k_0^3}{(2\pi)^4} |\hat{\boldsymbol{y}} + \hat{\boldsymbol{z}}|. \qquad (22)$$

which is closely related to the Jacobian J above. Here the factor of k_0^3 corresponds to three-dimensional imaging.

The associated point-spread function is

$$I_{k_0}(\boldsymbol{p}) \quad = \int \chi_{2k}(\boldsymbol{\xi}) e^{i\boldsymbol{\xi}\cdot(\boldsymbol{p}-\boldsymbol{x})}\, d^3\xi\ q(\boldsymbol{x})\, d^3x \qquad (23)$$

where χ_{2k} denotes the function that is one inside the ball of radius $2k$ and zero outside.

D. Moving Target Tomography.

Moving Target Tomography [7] models the signal using a simplified version of (5). For this simplified model, our imaging formula (10) reduces to matched-filter processing [7] with a different filter for each location $\boldsymbol{p}$ and for each possible velocity $\boldsymbol{u}$.

VI. Conclusion

We see from (14) that the point-spread function for phase-space imaging is a weighted coherent sum of bistatic radar ambiguity functions.

It remains to analyze this point-spread function and determine whether ambiguities are present in phase-space imaging.

Acknowledgment

This work was supported by the Office of Naval Research, by the Air Force Office of Scientific Research[1] under agreement number FA9550-06-1-0017, by Rensselaer Polytechnic Institute, and by the National Research Council.

[1]Consequently the U.S. Government is authorized to reproduce and distribute reprints for Governmental purposes notwithstanding any copyright notation thereon. The views and conclusions contained herein are those of the authors and should not be interpreted as necessarily representing the official policies or endorsements, either expressed or implied, of the Air Force Research Laboratory or the U.S. Government.

References

[1] N. Bleistein, J.K. Cohen, and J.W. Stockwell, *The Mathematics of Multidimensional Seismic Inversion,* New York: Springer, 2000)

[2] B. Borden and M. Cheney, "Synthetic-Aperture Imaging from High-Doppler-Resolution Measurements," *Inverse Problems,* **21**, pp. 1–11 (2005).

[3] M. Cheney and B. Borden, "Imaging Moving Targets from Scattered Waves," *Inverse Problems* 24 (2008) 035005.

[4] C.E. Cook and M. Bernfeld, *Radar Signals,* New York: Academic Press, 1967.

[5] A.J. Devaney, "Inversion formula for inverse scattering within the Born approximation," Optics Letters, **7**, pp. 111–112 (1982).

[6] A.J. Devaney, "A filtered backpropagation algorithm for diffraction tomography", Ultrasonic Imaging, **4**, pp. 336–350 (1982).

[7] B. Himed, H. Bascom, J. Clancy, and M.C. Wicks, "Tomography of Moving Targets (TMT)", in *Sensors, Systems, and Next-Generation Satellites V.*, ed. H. Fujisada, J.B. Lurie, and K. Weber, Proc. SPIE Vol. 4540 (2001) pp. 608 – 619.

[8] N. Levanon, *Radar Principles,* New York: Wiley, 1988.

[9] C.J. Nolan and M. Cheney, "Synthetic Aperture Inversion," Inverse Problems, **18**, pp. 221–36 (2002)

[10] N.J. Willis, *Bistatic Radar*, Norwood, MA: Artech House, 1991.

[11] N.J. Willis and H.D. Griffiths, *Advances in Bistatic Radar*, Raleigh, North Carolina: SciTech Publishing, 2007.

[12] N.J. Willis, "Bistatic Radar," in *Radar Handbook*, M. Skolnik, ed., New York: McGraw-Hill, 1990.

[13] B. Yazici, M. Cheney, and C.E. Yarman, "Synthetic-aperture inversion in the presence of noise and clutter", Inverse Problems **22**, pp. 1705-1729 (2006) .